Desalination and Water Treatment
www.deswater.com

doi: 10.5004/dwt.2021.26615

211 (2021) 304–318
January

Prediction of RSM and ANN in the decolorization of Reactive Orange 16 using biochar derived from *Ulva lactuca*

M. Kumar[a,*], S. Sujatha[b], R. Gokulan[c,*], A. Vijayakumar[c], S. Praveen[d], S. Elayaraja[e]

[a]*Department of Civil Engineering, Government College of Technology, Coimbatore, Tamil Nadu – 641 013, India, Tel. +91-9952711014; email: kumargeo_77@gct.ac.in*
[b]*Department of Civil Engineering, K. Ramakrishnan College of Technology, Trichy, Tamil Nadu – 621 112, India, email: sujalalit@gmail.com*
[c]*Department of Civil Engineering, GMR Institute of Technology, Rajam, Andhra Pradesh – 532 127, India, Tel. +91-9944233081; emails: gokulravi4455@gmail.com/gokulan.r@gmrit.edu.in (R. Gokulan), vijayakumarkct@gmail.com (A. Vijayakumar)*
[d]*Department of Civil Engineering, Anna University, University College of Engineering Ramanathapuram, Ramanathapuram 623 513, Tamil Nadu, India, email: praveensarvan@gmail.com*
[e]*Department of Civil Engineering, PSG Institute of Technology and Applied Research, Coimbatore, Tamil Nadu – 641 062, India, email: elayaraja86@gmail.com*

Received 20 April 2020; Accepted 18 September 2020

ABSTRACT

The present research compares the prediction of the response surface methodology (RSM) and artificial neural network (ANN) on the decolorization of Reactive Orange 16 (RO16) using a novel adsorbent produced from *Ulva lactuca* (seaweed). These mathematical models were designed based on four process conditions biochar dose, pH, temperature, and initial concentration. The experimental trials concluded that the dye removal of 93.10% was achieved at an optimum biochar dosage of 2 g/L, pH of 2, initial concentration of 0.5 mmol/L, and temperature of 40°C. The biochar characterization confirmed the presence of functional groups that are responsible for the adsorption of dye. The mathematical predictive model of RSM and ANN was compared with the experimental trials and a correlation coefficient (R^2) of 0.95 is obtained for RSM, whereas a correlation coefficient (R^2) of 0.99 was obtained for ANN. ANN prediction model was far better than RSM in the prediction of decolorization of Reactive Orange 16 (RO16) using *U. lactuca* as a novel adsorbent. The adsorption isotherm studies concluded that four parameter model Fritz–Schlunder – IV and Marczewski–Jaroniec were found to best fit with a correlation coefficient of 0.9999. Pseudo-second-order kinetic model was found to best fit the experimental data.

Keywords: Artificial neural network; Biochar; Decolorization; Reactive Orange 16 (RO16); Response surface methodology

1. Introduction

Pollutants in the form of dyes from the textile industry were one of the hazardous materials that affect the environment if it is not treated properly. Since, if it enters into the nearby water streams or the wastewater it will react immediately and become more stable and it is difficult to degrade since it is more complex [1]. These dyes are toxic, carcinogenic compounds that are present in the dyes will affect the microorganism, aquatic life and also it will affect the surface and groundwater that in turn will affect the health of the human being if it is not treated properly [2]. Even 1 mg/L of dyes in water will affect the quality of the water and causes a serious impact on health. So, it is to be treated properly using physical, chemical, or biological methods.

* Corresponding authors.

Many physical, chemical, and biological methods are used for the degradation of dyes from the water or wastewater [3]. But in physical and chemical methods the pollutants are not degraded, it is converted into other forms and creates the secondary pollutants to the environment if it is not disposed of properly [4]. So recently many researchers are concentrating on the biological methods to degrade the dyes and to avoid the secondary pollutants to the environment [5]. Some of the commonly used biological methods are biosorption, bioaccumulation, and phytoremediation. Biological methods use biomaterials that are organic or inorganic that are capable of adsorbing or degrading the toxic wastes materials. Of these biological methods, biosorption plays a key role in the removal of dyes. A biomaterial-based sorbent is produced from biological materials and that is used in the adsorption.

In the past, commonly used sorbents were produced from cocoa pod husk [6], coconut shell [7], date palm rachis [8], jujube stones [8] in the form of activated carbon and commercial activated carbon [9] also used in the adsorption process. Similarly, agricultural solid wastes like bark [10], cocoa pod husks [11], coconut husk [12], coconut shells [13,14], groundnut shell [15], rice husk [16], sawdust [17], breadfruit peel [18], and *Artocarpus camansi* peel [19]. Industrial wastes like activated sludge [20], bio fly ash [21], chitin [22], chitosan [23], commercial chitosan powder [24], fly ash [25], industrial waste sludge [26], metal hydroxide sludge [27], paper mill sludge [28], red mud [29], tannery sludge [30], ceramic adsorbents [31], and cedar [32]. Natural material clays like acid-activated clay [33], natural bentonite [34], sepiolite [35], synthetic talc, and zeolite [36]. Biological materials like *Amphiroa foliacea* [37], *Bacillus megaterium* [38], *Candida lipolytica* [39], *Corynebacterium glutamicum* [40], *Laminaria* sp. (protonated with HCl) [41] *Pseudomonas* [42] *Phanerochate chrysosporium* [43], and enriched microorganism compost as adsorbents [44]. Recently seaweeds like *Ulva lactuca*, *Ulva reticulata*, *Caulerpa Scalpelliformis* [45–48], *Sargassum wightii*, *Turbinaria conoides* [49], and *Kappaphycus alvarezii* [50] are also used as a prominent adsorbent. Biochar is a carbon-rich biomaterial that is produced in the absence of oxygen [51]. A limited study has been carried out in the application of biochar as a successful adsorbent material.

Many mathematical tools are developed for the optimization of the experimental trails. Response surface methodology (RSM) and artificial neural network (ANN) are such types of optimization tools that can be utilized as a predictive tool [52]. RSM is a method in which dependent variables are compared with various independent variables at different levels using statistical and mathematical methods that are applied based on the experimental data [53–55]. Accordingly, RSM can also avoid repeating a greater number of experimental trails, in turn, reduces the time and cost associated with the testing [56,57]. Nowadays, ANNs is used as one of the best prediction models in learning algorithms and understanding the link between the input and output variables for nonlinear systems [58–63]. In recent times, RSM and ANN models are compared with experimental trails by different authors [64–66]. Hence in the current research novel adsorbent biochar was produced from *U. lactuca* for the decolorization of Reactive Orange 16 (RO16) in batch mode operation under optimum conditions. To the best of our knowledge, this is the first research of utilizing biochar derived from *U. lactuca* species for the decolorization of Reactive Orange 16 (RO16).

2. Materials and methods

2.1. Seaweed and chemical

The marine seaweed *U. lactuca* was collected from the seashore near Rameswaram, India. The collected seaweed was first rinsed with distilled water and natural drying was carried out for 24 h. Then the seaweed is reduced into a uniform size of 0.75 mm. The dyes used in this study are Reactive Orange 16 (RO16) and it was procured from Sigma Aldrich (India). The empirical formula of Reactive Orange 16 (RO16) is $C_{20}H_{17}N_3Na_2O_{11}S_3$ with a molecular weight of 617.54 g/mmol. The λ_{max} value of Reactive Orange 16 (RO16) is 490 nm. The structure of RO16 is shown in Fig. 1.

2.2. Synthesis of biochar and characterization of biochar

A measured quantity of 50 g of the dried biomass (seaweed) is utilized for the synthesis of biochar. A muffle furnace with a heating rate of 5°C/min was used for the thermal pyrolysis. The thermal pyrolysis was carried out at an oxygen-free environment at different temperatures such as 300°C, 350°C, 400°C, 450°C, and 500°C. Before the start of the experiments, the muffle furnace was purged with nitrogen gas to ensure an oxygen-free environment inside the muffle furnace [67]. At each temperature, three trials were carried out to determine the yield of the biochar. The yield of the biochar is taken in terms of mass. From the experimental investigation, it was concluded that the biochar yield is maximum at a temperature of 300°C and it is carried out for further studies.

2.3. Batch adsorption studies

A rotating orbital shaker with operating conditions of 160 rpm for 6 h was used for batch studies. The effect of adsorption process was studied by varying the parameters such as biochar dosage, equilibrium pH, initial concentration, and temperature at different levels. Once the batch studies were completed, a centrifuge with an operating condition of 2,400 rpm for 10 min was used to separate the supernatant and pellet. The collected supernatant is used for further studies.

2.4. Design of experiments

2.4.1. Response surface methodology

For this study, Box–Behnken design (BBD) was used for modeling. The regression analysis and design of experiments are done by using Minitab software (version 16.1.1). Table 1 shows the BBD design with actual and coded values of the variables with three different levels of high, medium, and low (–1, 0, +1). The BBD was analyzed using a quadratic equation as shown in Eq. (1).

$$Y = \beta_0 + \sum_{i=1}^{k} \beta_i x_i + \sum_{i=1}^{K} \beta_{ii} x_i^2 + \sum_{i=1} \sum_{j=i+1} \left(\beta_{ij} x_i x_{ij} + \varepsilon \right) \quad (1)$$

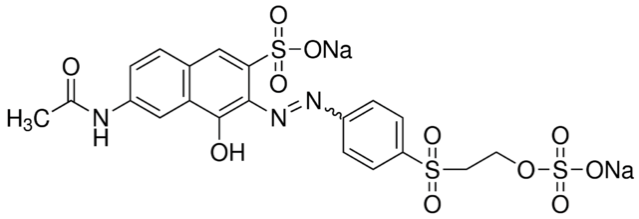

Fig. 1. Structure of Reactive Orange 16 (RO16).

Table 1
BBD design variable levels

Coded variable levels			
1	0	–1	Variables
2	4	6	Biochar dosage (g/L)
2	3	4	Equilibrium PH
0.25	0.50	1.0	Initial concentration (mmol/L)
25	35	45	Temperature (°C)

where Y is the response (% removal), β is a regression coefficient. Where x_i and x_j are independent variables and ε is the error.

2.4.2. ANN model

A feed-forward backpropagation neural network algorithm with two layers was used. For this study, the neural network toolbox of MATLAB Software version was used to predict the removal efficiency of dyes. A Levenberg–Marquardt backpropagation (LMA) algorithm was used with two layers (Fig. 2). A total of 27 data samples were used and divided into 70% training (21 samples), 15% validation (4 samples), and 15% test (4 samples), respectively. The data set of different process conditions were normalized between limits of –1 and 1 using Eq. (2).

$$x_{ik} = 0.8 \times \frac{\max y_i(k) - y_i(k)}{\max y_i(k) - \min y_i(k)} + 0.1 \quad (2)$$

where x_{ik} is the normalized value of response k of trail i, max $y_i(k)$ is the maximum value of y_ik, $y_i(k)$ is the response k of the trail I, min y_ik is the minimum value of y_ik (i = 1, 2, …. n), and I is the number of experiment trails.

3. Result and discussion

3.1. Biochar characterization

Fig. 3 shows the scanning electron microscopy (SEM) of *U. lactuca*-biochar and RO16 bounded biochar. For instance, the biochar surface was identified with different sized uneven pores and this may be due to the pyrolysis. Pyrolysis resulted in the uneven surface and this may increase the specific surface area, which increased the binding capacity. So, the sorbent produced from *U. lactuca* can be used as a successful adsorbent. Robic et al. [68] reported that *U. lactuca* is composed of water-soluble *ulvan* and

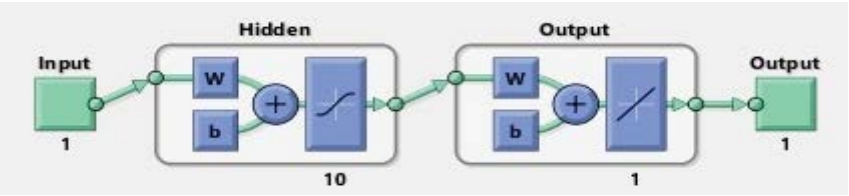

Fig. 2. ANN-based neural network model.

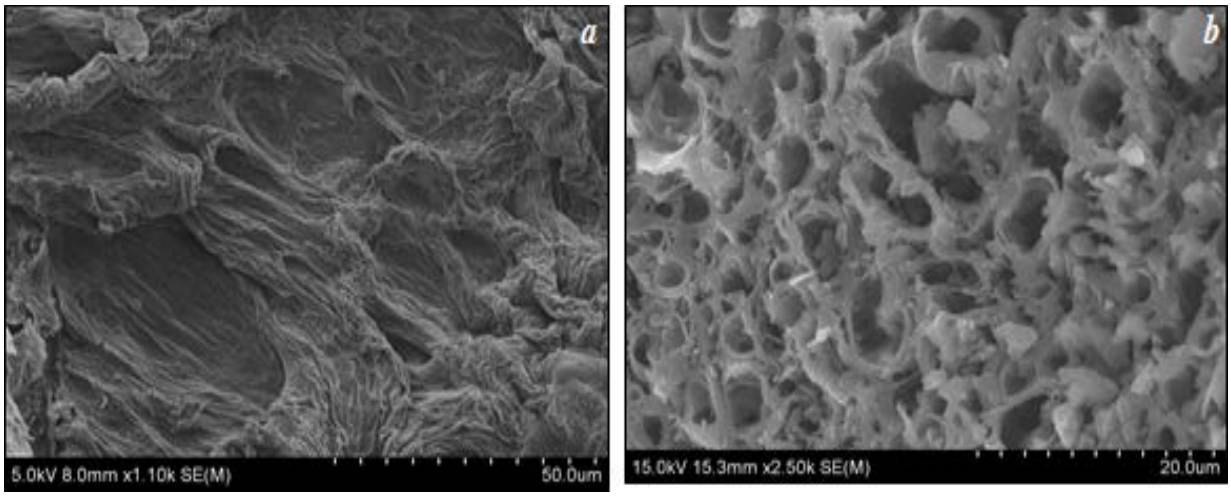

Fig. 3. Scanning electron microscopy of raw biochar (a) and RO16 loaded biochar (b).

the remaining 38%–54% is composed of cell wall polysaccharides (on a dry weight basis). The SEM images (Fig. 3) also pointed out that there is much difference in the biochar surface and indicates that cation and anion exchange happened between the dye and the biochar surface.

Fig. 4 demonstrates the Fourier transform infrared (FT-IR) spectrum of the *U. lactuca*-derived biochar and RO16 loaded biochar. From Fig. 4, it is clear that a major shift has occurred from a strong band at 1,072–1,073 of (C–O (alcohol) band), 1,411–1,418 (C=O, symmetric), 1,628–1,625 (C=O stretch of COOH, asymmetric), 2,914–2,919 (C–H stretch), and 3,427–3,442 (–NH, –OH stretching) [69,70]. Therefore, it was obvious that biochar comprises binding sites of different nature which exhibited the above-mentioned spectral peaks. This is due to the exchange of other ions present on the surface of the biochar by Remazol dyes during adsorption. This shows the involvement of numerous functional groups on the biochar matrix. Therefore, the FT-IR spectra of biochar bounded with Remazol dyes exhibited substantial deviations in biochar functional sites after exposed to Remazol dyes (Fig. 4).

3.2. RSM based predictive model

The developed equation for the dye removal using an RSM is given in Eq. (3).

$$\begin{aligned}\%\ \text{Removal} = {} & 69.75 + 9.379A + 8.31B + 15.70C - 0.945D - \\ & 0.5365A^2 - 0.896B^2 - 24.73C^2 + 0.01717D^2 - \\ & 0.4625AB - 1.250AC - 0.0900AD - 2.700BC + \\ & 0.0200BD + 0.520CD \end{aligned} \quad (3)$$

where A is the biochar dose (g/L), B is the pH, C is the initial concentration (mmol/L), and D is the temperature (°C).

Fig. 5 shows the Pareto chart of the standard effects of different variables with different combinations. The reference line at a standardized effect at 2.18 denotes 0.05 significant levels with a 95% confidence level. The variables which

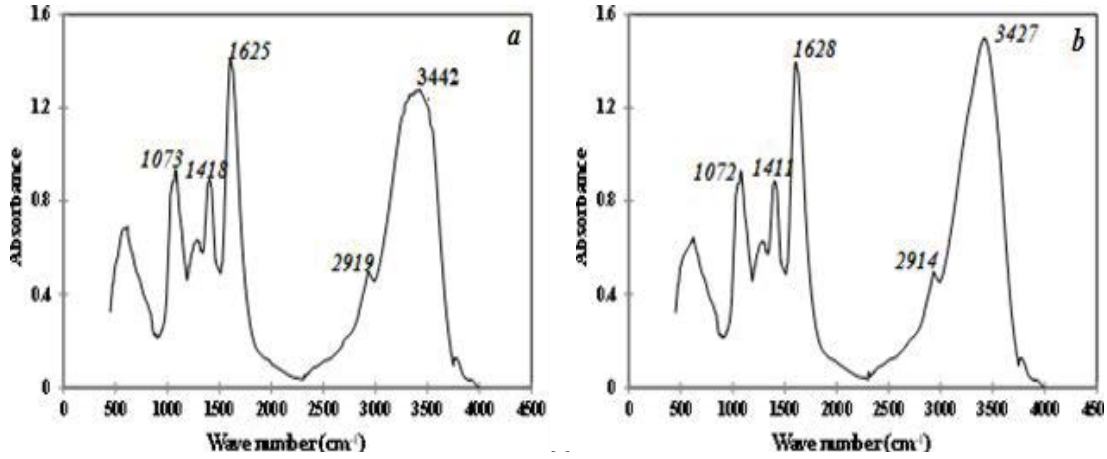

Fig. 4. FT-IR spectra of RO16-loaded biochar (a) and raw biochar (b).

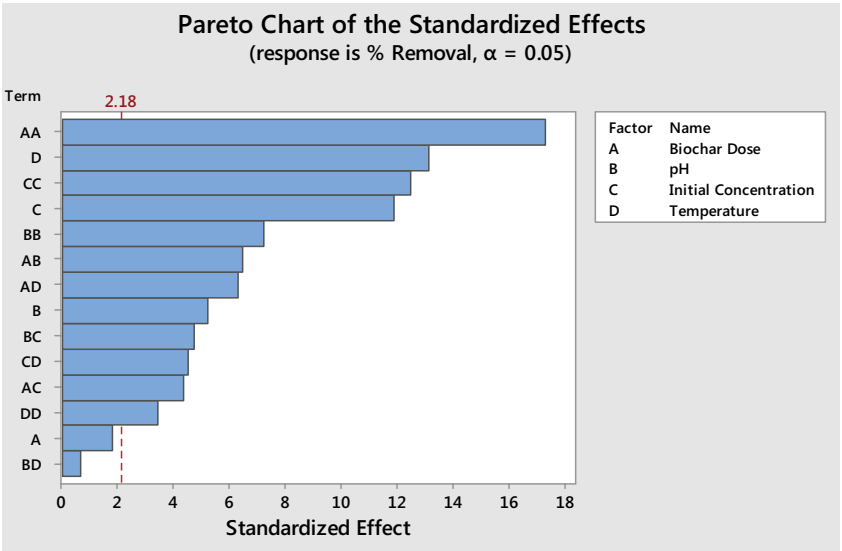

Fig. 5. Pareto chart of the standard effects predicted by RSM.

are greater than the standard effect of 2.18 (reference line) are statistically significant and variables that are less than the standard effect of 2.18 are not statistically significant. From Fig. 5, it is evident that the independent variable *A* (biochar dose) and interaction variables *BD* (pH × temperature) are not statistically significant, whereas remaining all variables are statistically significant. A maximum significant level was observed for *AA* (Biochar × Biochar). Fig. 6 shows the residual plots for dye removal efficiency. Table 2 summarized the analysis of variance for % removal of Reactive Orange.

3.2.1. Effect of process conditions

Fig. 7 shows the 3D surface plot and 2D contour plots for two different independent parameters with respect to the removal % of the dye. A 2D contour plot was used to explore the relationship between three variables in two-dimensional relationships by fixing the % removal as the target and any two process conditions were compared in two dimensional. Similarly, 3D surface plot or 2D wireframe plot is a three-dimensional plot that compares target (% removal) in the *z*-axis and any of the two process conditions in the *x* and *y*-axis. That target or response is represented in the form of a surface plot or wireframe plot.

Figs. 7a–e shows the surface and contour plot of two variables temperature and biochar with respect to the response (% removal). From Figs. 7a–c and e, it is evident that the contour plot is following a stationary ridge pattern. The stationary ridge pattern of the contour plot implies that other parameters affect the response in maximum. It is also noted that temperature is the common variable in these contour plots and it shows that temperature is not having a maximum effect on the response. From the surface plot and contour plot, it is concluded that the maximum response of 91.80% was achieved at a temperature of 40°C at a biochar dose of 2 g/L. Similarly, >91.80% was achieved at a pH of 4 and a temperature of 40°C, >91.80% was achieved at an initial concentration of 0.25 mmol/L and temperature of 40°C and >91.80% was achieved at an initial concentration of 0.25 mmol/L and pH of 4. So, it can be concluded that the optimum temperature for the maximum removal of dye is 40°C.

Fig. 7d shows the surface plot and contour plot of initial concentration and biochar dosage with respect to % removal. The contour plot follows a simple maximum pattern. According to this pattern, the color gets darker when it reaches maximum. From Fig. 7d, it is evident that the maximum response (>91.80%) was attained at a biochar dosage of 4 g/L with an initial concentration of 0.50 mmol/L. Fig. 7f shows the surface plot and contour plot of initial concentration and biochar dosage with respect to % removal. The contour plot follows a rising ridge pattern. From Fig. 7f, it is evident that the response increases as we decrease the pH and increase with an increase in biochar dosage.

3.3. ANN-based predictive model

Fig. 8a shows the error histogram with 20 bins predicted by an ANN. ANN validates the experimental data and predicts the response. There will be always an error between the predicted response and the experimental data until $R^2 = 1$. The residual error between each observation is predicted and a range is fixed. ANN predicted the maximum error of 0.12 for observation 06 and nil error is predicted

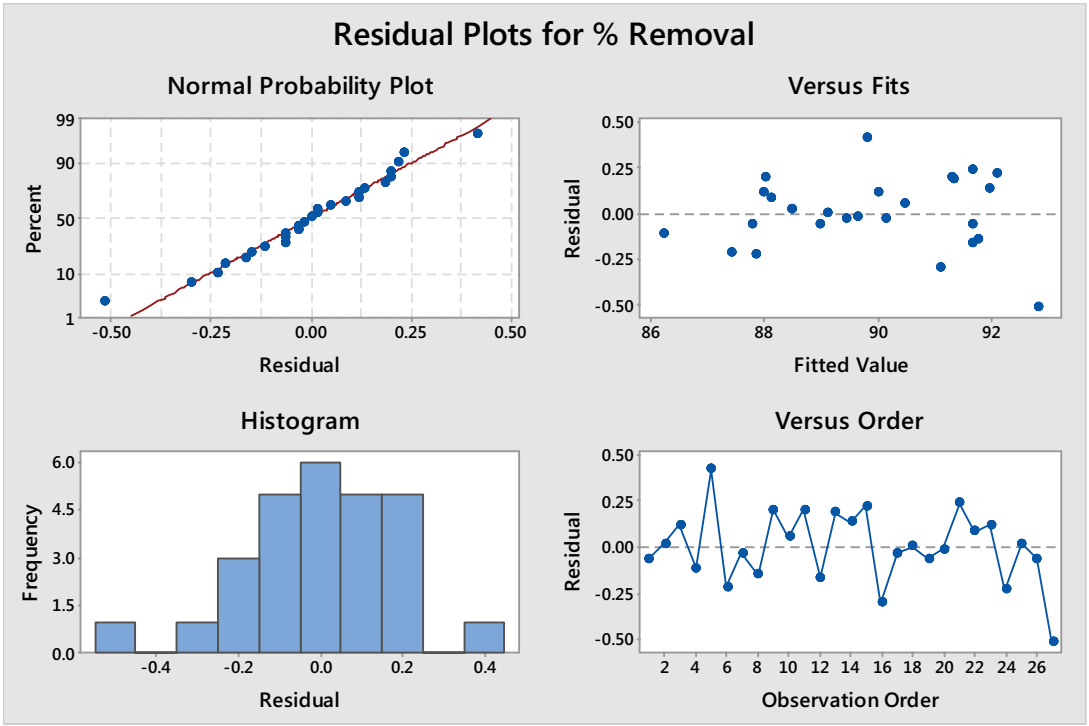

Fig. 6. Residual plots for % removal predicted by RSM.

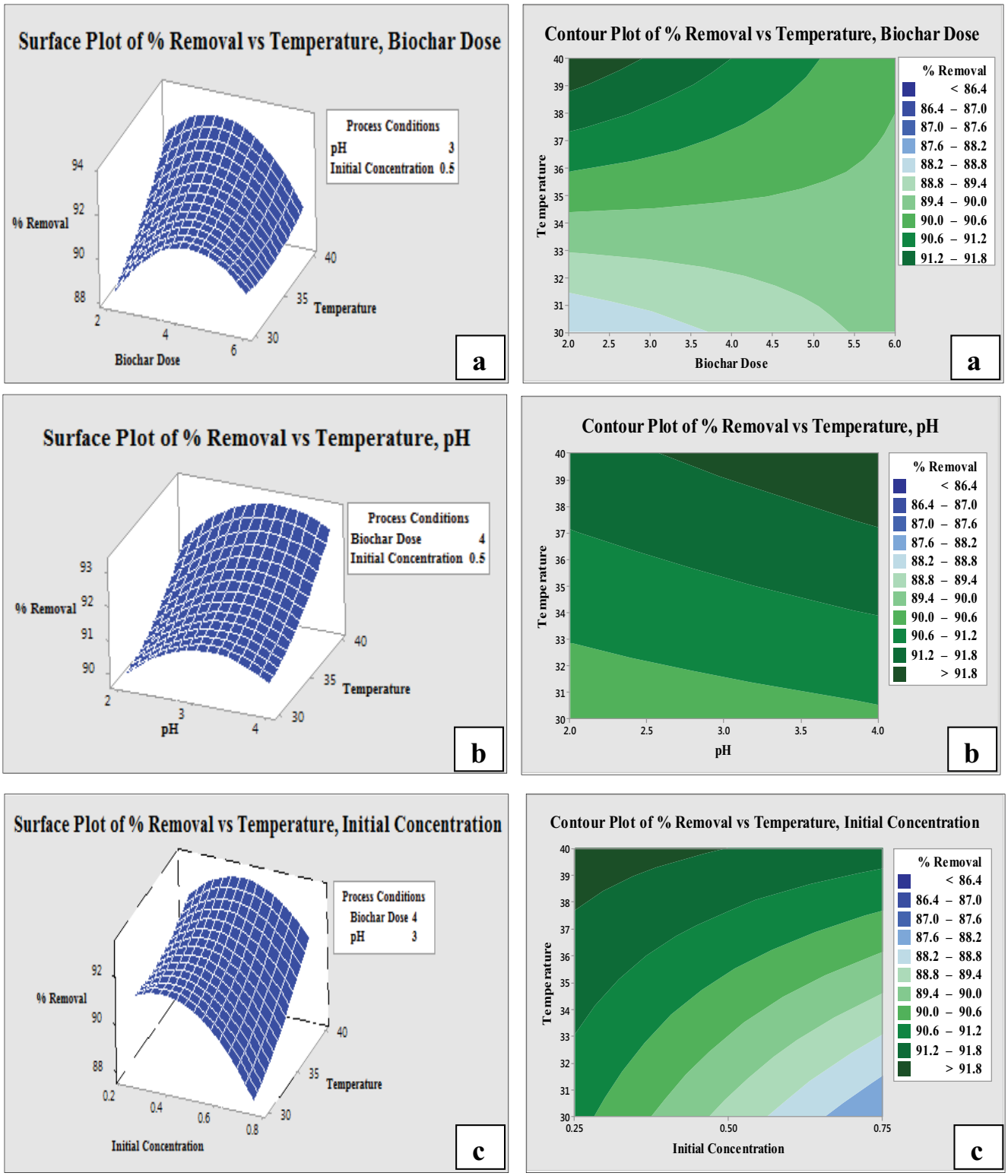

Fig. 7. Continued

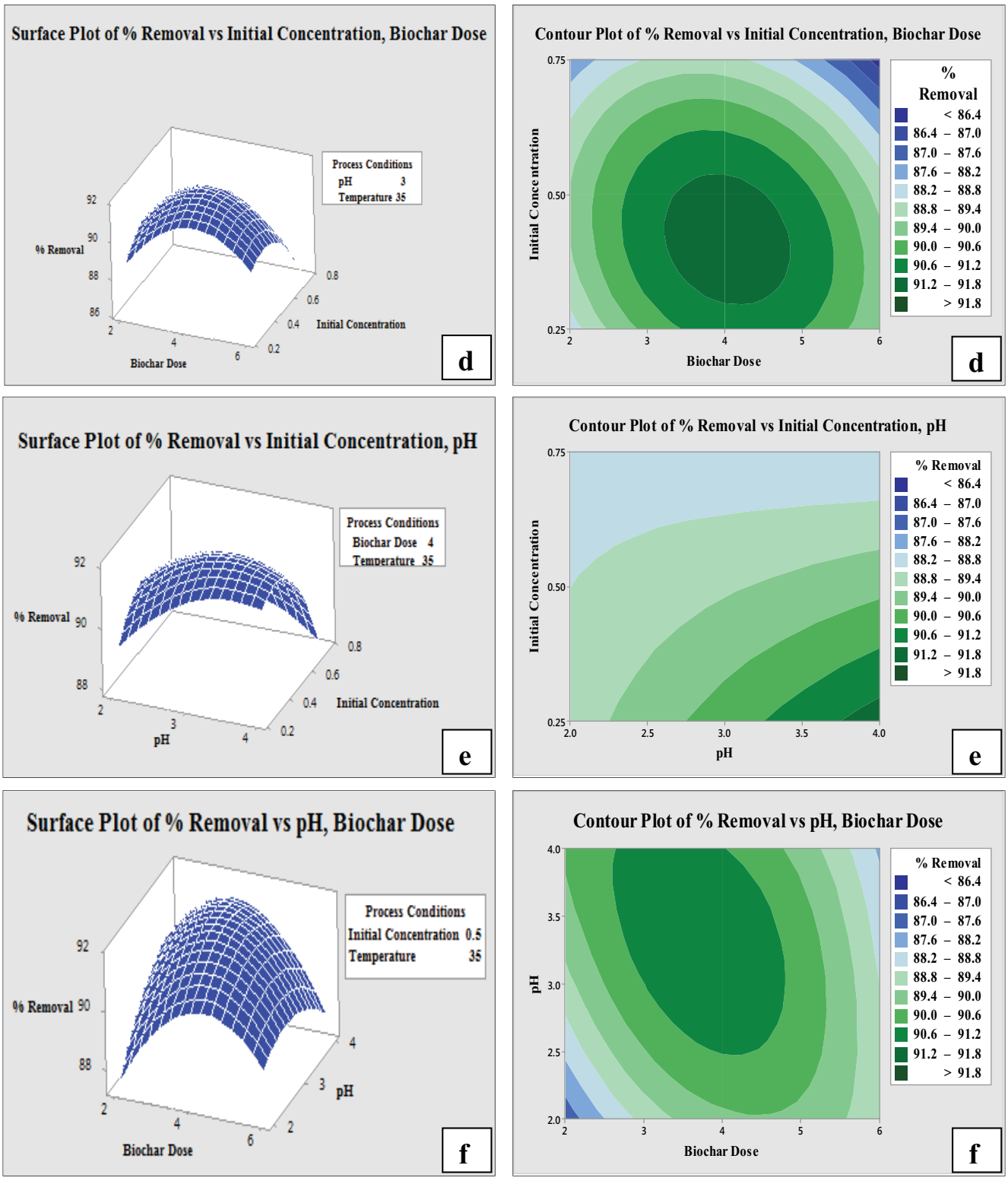

Fig. 7. Surface plot and contour plots of; % removal vs. temperature and biochar dosage (a), % removal vs. temperature and pH (b), % removal vs. temperature and initial concentration (c), % removal vs. initial concentration and biochar dosage (d), % removal vs. initial concentration and pH (e), and % removal vs. pH and biochar dosage (f).

Table 2
Analysis of variance for % removal of Reactive Orange 16

Source	DF	Adj. SS	Adj. MS	*F*-value	*P*-value
Model	14	80.7791	5.7699	70.53	0.000
Linear	4	28.2100	7.0525	86.21	0.000
Biochar dose (*A*)	1	0.2700	0.2700	3.30	0.094
pH (*B*)	1	2.2533	2.2533	27.54	0.000
Initial concentration (*C*)	1	11.6033	11.6033	141.84	0.000
Temperature (*D*)	1	14.0833	14.0833	172.16	0.000
Square	4	40.7916	10.1979	124.66	0.000
Biochar dose × biochar dose (A^2)	1	24.5579	24.5579	300.20	0.000
pH × pH (B^2)	1	4.2801	4.2801	52.32	0.000
Initial concentration × initial concentration (C^2)	1	12.7445	12.7445	155.79	0.000
Temperature × temperature (D^2)	1	0.9823	0.9823	12.01	0.005
2-Way interaction	6	11.7775	1.9629	23.99	0.000
Biochar dose × pH (*AB*)	1	3.4225	3.4225	41.84	0.000
Biochar dose × Initial concentration (*AC*)	1	1.5625	1.5625	19.10	0.001
Biochar dose × Temperature (*AD*)	1	3.2400	3.2400	39.61	0.000
pH × initial concentration (*BC*)	1	1.8225	1.8225	22.28	0.000
pH × temperature (*BD*)	1	0.0400	0.0400	0.49	0.498
Initial concentration × Temperature (*CD*)	1	1.6900	1.6900	20.66	0.001
Error	12	0.9817	0.0818	–	–
Lack-of-fit	10	0.8950	0.0895	2.07	0.370
Pure error	2	0.0867	0.0433	–	–
Total	26	81.7607	–	–	–
R^2 = 98.80%	R^2 (Adj.) = 97.40%		R^2 (Predicted) = 93.46%		

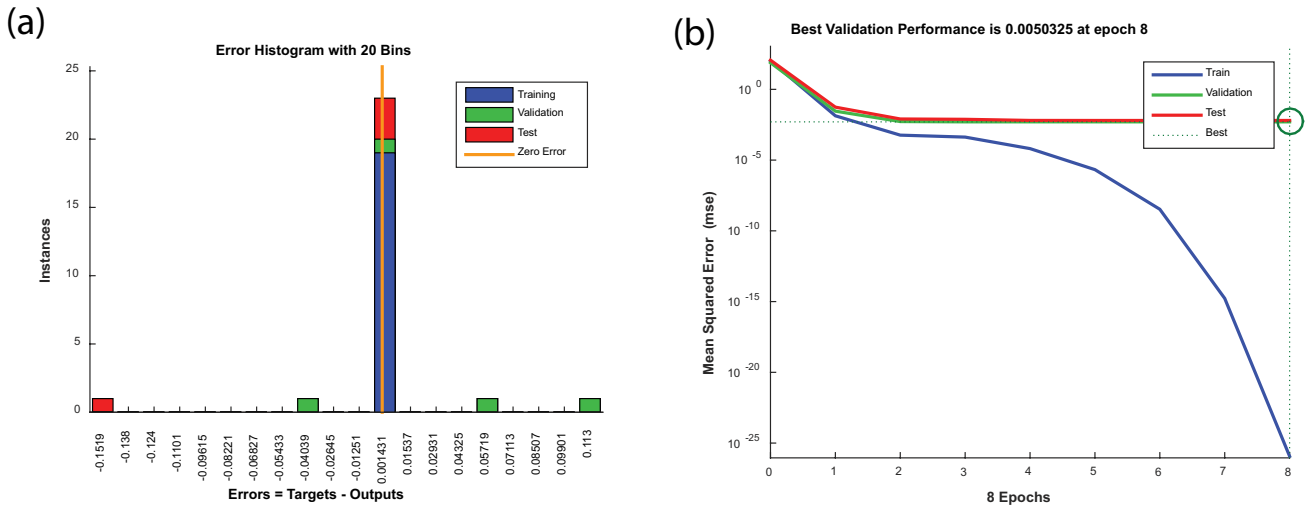

Fig. 8. Error histogram for % removal predicted by ANN (a) and MSE for train, validation, and testing (b).

for many observations. Fig. 8a shows the histogram of 20 bins with a total error of 2.26. So, the error for each bin is 0.113 or the difference between each bin is 0.113. The training was stopped with a mean square error of 0.005 at epoch 8 (Fig. 8b) and which is very close to the acceptable limit. Almost 23 observations that are validated by ANN showed nil error. This shows that the predicted responses by ANN are close to experimental trails.

Lim and Lee [71] reported that the Levenberg–Marquardt backpropagation algorithm can obtain higher R^2 value with lower standard deviation and MSE than any other algorithm. The optimum network topology of ANN is 4:10:1, which shows, that four input variables with ten hidden neurons and a single output variable. Fig. 9 shows the R^2 value of the experimental and predicted response of ANN. The R^2 value of 1, 0.9997, 0.9989, and 0.9997 was obtained

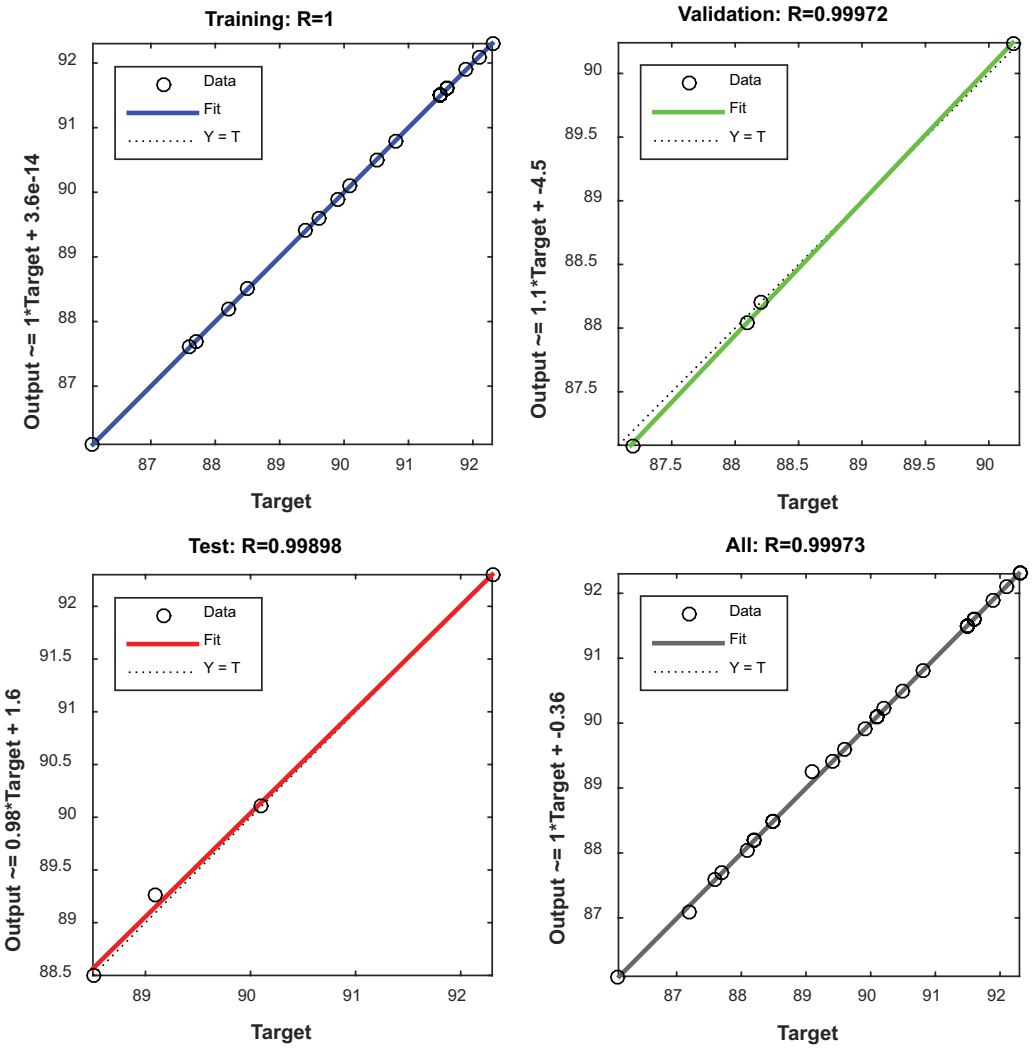

Fig. 9. ANN predicted values based on experimental values.

for training, validation, testing, and all. The predicted response of ANN shows that the removal efficiency of dye is in good agreement with the experimental trails. Therefore, it is concluded that ANN is the best predictive model than the RSM predictive model and for further adsorption studies the developed ANN model can be used for different combinations.

3.4. Comparison between experimental, RSM, and ANN predictive model

Table 3 summarizes the predicted response and error of RSM and ANN with experimental data. From Table 3, for most of the observation, the error is nil for ANN, which shows that the predicted response by ANN is in good agreement with the experimental removal efficiency.

3.4.1. Box plot of experimental and predictive model

Fig. 10 shows the boxplot of response obtained by experimental, RSM, and ANN predictive model. From the graph, it is also concluded that the response obtained by experiments is close with the response predicted by ANN then the response predicted by RSM. The median value for an experiment, RSM and ANN are 90.10, 89.78, and 90.10. So, from the boxplot it is concluded that the predicted response obtained by ANN is in good accordance with the experimental studies then, the predicted response by RSM, and for further studies the ANN predictive model was used.

3.4.2. Hierarchical cluster analysis

Fig. 11 shows the hierarchical cluster analysis (HCA) for experimental, RSM, and ANN. Cluster analysis was carried out by single-linkage methods that are used to find the distance and similarity between the closely associated variables. From the dendrogram (Fig. 11), it is clear that a cluster was formed between the experimental and ANN with a similarity level and distance level of 68.51 whereas a cluster between experiment and RSM showed a similarity and distance level of 3.47 and. so, HCA proves that ANN predictive model is the best model for experimental data than the RSM predictive model.

Table 3
BBD matrix for process parameters with experimental, RSM and ANN predicted % removal of Reactive Orange 16

Run	*A*	*B*	*C*	*D*	Removal %			Error	
	Biochar dose	pH	Initial concentration	Temperature	Experimental	RSM predicted	ANN predicted	RSM	ANN
1	2	3	0.75	35	87.70	87.77	87.70	–0.07	0.00
2	4	2	0.75	35	88.50	88.48	88.50	0.02	0.00
3	6	3	0.50	40	90.10	89.98	90.10	0.12	0.00
4	6	3	0.75	35	86.10	86.22	86.10	–0.12	0.00
5	4	2	0.50	30	90.20	89.78	90.24	0.42	–0.04
6	2	2	0.50	35	87.20	87.42	87.08	–0.22	0.12
7	2	4	0.50	35	90.10	90.13	90.10	–0.03	0.00
8	4	2	0.50	40	91.60	91.75	91.60	–0.15	0.00
9	4	3	0.75	40	91.50	91.30	91.50	0.20	0.00
10	4	4	0.50	30	90.50	90.45	90.50	0.05	0.00
11	4	4	0.75	35	88.20	88.00	88.20	0.20	0.00
12	4	3	0.50	35	91.50	91.67	91.50	–0.17	0.00
13	4	4	0.25	35	91.50	91.32	91.50	0.18	0.00
14	4	3	0.25	40	92.10	91.97	92.10	0.13	0.00
15	2	3	0.50	40	92.30	92.08	92.30	0.22	0.00
16	4	3	0.25	30	90.80	91.10	90.80	–0.30	0.00
17	6	3	0.25	35	89.40	89.43	89.40	–0.03	0.00
18	4	2	0.25	35	89.10	89.10	89.26	0.00	–0.16
19	6	2	0.50	35	88.90	88.97	89.90	–0.07	0.00
20	6	3	0.50	30	89.60	89.62	89.60	–0.02	0.00
21	4	3	0.50	35	91.90	91.67	91.90	0.23	0.00
22	2	3	0.50	30	88.20	88.12	88.20	0.08	0.00
23	6	4	0.50	35	88.10	87.98	88.04	0.12	0.06
24	4	3	0.75	30	87.60	87.83	87.60	–0.23	0.00
25	2	3	0.25	35	88.50	88.48	88.50	0.02	0.00
26	4	3	0.50	35	91.60	91.67	91.60	–0.07	0.00
27	4	4	0.50	40	92.30	92.82	92.30	–0.52	0.00

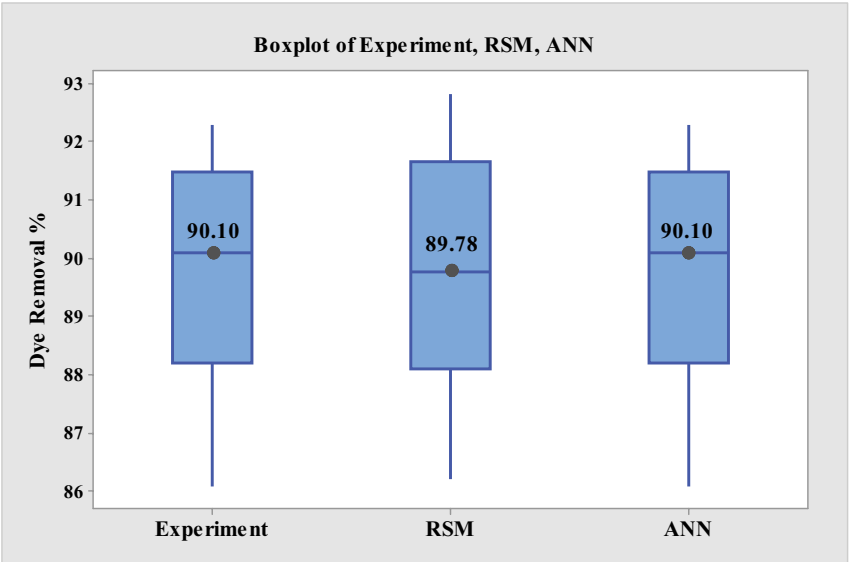

Fig. 10. Boxplot of experimental, RSM, and ANN models.

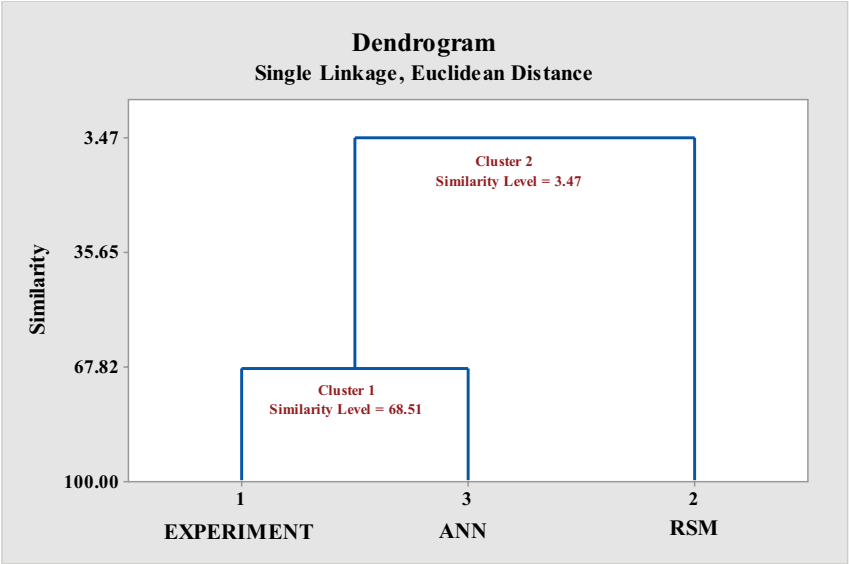

Fig. 11. Hierarchical cluster analysis of experimental, RSM, and ANN models.

3.5. Response optimizer

Fig. 12 shows the prediction of dye removal % by using a response optimizer. From the experimental studies, it is concluded that a maximum of 92.30% of the dye was removed with a process condition of biochar dose of 2 g/L, pH of 3, initial concentration of 0.5 mmol/L, and temperature of 40°C. Response optimizer predicted that maximum removal of 93.52% can be obtained at a process condition of biochar dose of 3.33 g/L, pH of 3.53, and initial concentration of 0.46 mmol/L, and temperature of 40°C. Three trails of experimental trials were carried out with the process condition optimized by response optimizer. The dye removal efficiency of 93.30%, 93.20%, and 93.40% was obtained at three different trails.

3.6. Adsorption mechanism

To understand the adsorption mechanism prediction of the rate-determining step is important. Commonly, solid–liquid adsorption is influenced by either external diffusion or intraparticle, or in some conditions both can happen. The adsorption mechanism can follow the three-step process as discussed below. First, it may be due to film diffusion, the movement of metals ions from the bulk solution to the external surface of the adsorbent. Second, it may be due to particle diffusion, metal ions will move to the interior to the adsorbents. Third, it may be adsorption, the metal ions move deep in the pores and binding spaces of the adsorbent. Isotherm model plays a very important role in understanding the adsorption mechanism. The experimental data were fitted with two, three, and four-parameter model. Based on the correlation coefficient R^2 the best fit of the two-parameter model was found to be in the order of Langumir > Freundlich > Smith. The Langmuir model with a correlation coefficient of 0.9817 and it shows that the homogenous and monolayer adsorption of RO16 on to biochar. The Freundlich isotherm was found to be partially fit with the experimental data with a correlation

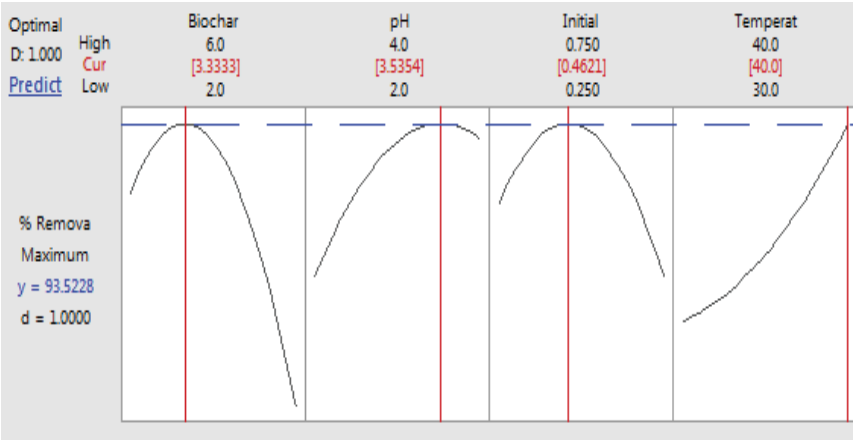

Fig. 12. Response optimizer for experimental trails.

coefficient (R^2) of 0.8578. This proved that to a certain extent that, the adsorption is heterogeneous and the values of $1/n_F < 1$ show that the cooperative adsorption. The ability of the three-parameter model to fit the experimental data was checked. From Table 4, it is concluded that the best fit model was in the order of Toth > Sips > Hill > Redlich–Peterson > Radke–Prausnitz > Unilin > Fritz–Schlunder – III > Vieth–Sladek > Khan. Even though the Toth model best fits the data the adsorption capacity was found to be less when compared to Hill, Khan, Vieth–Sladek, and Radke–Prausnitz. Among the four-parameter model both Fritz–Schlunder – IV and Marczewski–Jaroniec were found to best fit with a correlation coefficient of 0.9999. In overall, the four-parameter model best fits the experimental data when compared to the two and three-parameter model.

3.7. Kinetic study

The kinetic study was carried out by varying the initial concentration from 0.2 to 1 mmol/L and the final concentration was measure at a different time interval. From Fig. 13, it is concluded that the adsorption was maximum at the first 120 min followed by very little adsorption which occurred till 360 min. Almost 90% of the adsorption has occurred at 120 min and the optimum contact time for the adsorption is fixed was 120 min. Table 5 explores the pseudo-first-order and pseudo-second-order kinetic model parameters.

Table 4
Adsorption isotherm parameters for adsorption of RO16 onto *Ulva lactuca* derived biochar

Model	Parameter	Values	Model	Parameter	Values
		Two parameter model			
Freundlich	K_F	0.4633	Langmuir	Q_0	0.3404
	$1/n_F$	0.3365		b	31.6939
	R^2	0.8578		R^2	0.9817
Smith	WS1	0.0709			
	WS2	1.3837			
	R^2	0.7526			
		Three parameter model			
Redlich–Peterson	K_{RP}	7.9823	Vieth–Sladek	Q_{MVS}	0.6351
	α_{RP}	29.7744		B_{VS}	13.8926
	β_{RP}	1.2144		N_{VS}	1.3160
	R^2	0.9943		R^2	0.9891
Sips	K_S	84.8014	Radke–Prausnitz	Q_{MRP}	0.6351
	β_S	1.5186		K_{RP}	13.8929
	a_S	274.6297		n_{RP}	1.3160
	R^2	0.9966		R^2	0.9927
Toth	Q_{max}	0.2989	Fritz–Schlunder – III	Q_{MFS}	29.7748
	b_T	20.7270		K_{FS}	0.2681
	n_T	0.3469		N_{FS}	1.2144
	R^2	0.9997		R^2	0.9916
Hill	q_{mH}	0.3161	Unilin	Q_{MU}	29.8992
	n_H	1.4674		A_U	0.2690
	K_H	0.0047		B_U	1.2107
	R^2	0.9964		R^2	0.9918
Khan	Q_{max}	0.6139			
	b_k	10.3445			
	a_k	1.7743			
	R^2	0.8687			
		Four parameter model			
Fritz–Schlunder – IV	A_{FS}	4.7428	Marczewski–Jaroniec	Q_{MMJ}	0.2945
	a_{FS}	0.9364		K_{MJ}	18.7468
	B_{FS}	78.2681		N_{MJ}	3.8253
	B_{FS}	2.0337		M_{MJ}	0.9222
	R^2	0.9999		R^2	0.9999

Table 5
Kinetic parameters for adsorption of RO16 onto *Ulva lactuca* derived biochar

Kinetic model	Parameter	0.1 mmol/L	0.25 mmol/L	0.5 mmol/L	0.75 mmol/L	1 mmol/L
Pseudo-first-order kinetic model	Q_e	0.0452	0.1128	0.2244	0.2874	0.2904
	K_1	0.0615	0.0581	0.0475	0.0524	0.0650
	R^2	0.9847	0.9898	0.9918	0.9873	0.9841
Pseudo-second-order kinetic model	Q_e	0.0486	0.1214	0.2438	0.3107	0.3122
	K_2	2.1365	0.7957	0.3050	0.2731	0.3479
	R^2	0.9978	0.9967	0.9961	0.9954	0.9987

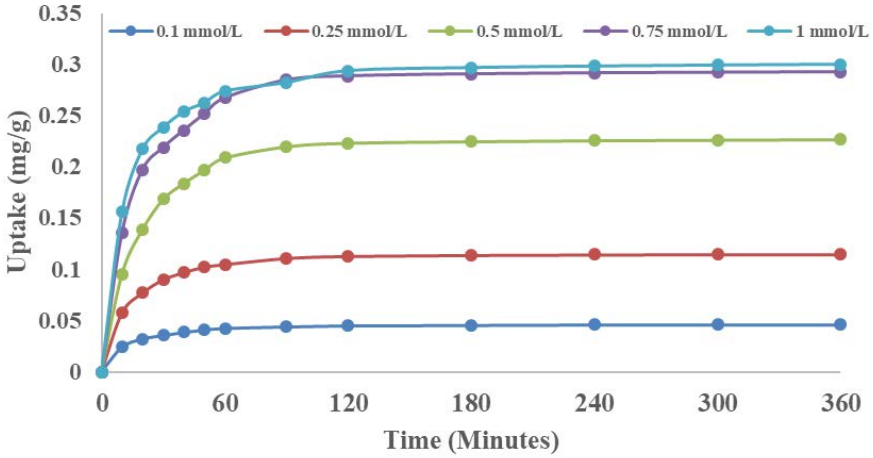

Fig. 13. Experimental uptake of RO16 during the kinetic study.

Pseudo-second-order kinetic model was found to be the best fit model with a correlation coefficient of not less than 0.9954. It also revealed that boundary layer thickness and external mass transfer strongly influenced the adsorption, without resistance to mass transfer within the pores of the sorbent. Moreover, adsorption on boundary layer is strongly governed by the electron-donor forces between these anionic dyes and positively charged biochar. This is agreeable with the results obtained from the effect of pH since the optimum pH for the removal of Remazol dyes is 2, which indicates the surface of the biochar is charged with positive ions (H+) that enhance the maximum removal efficiency.

4. Conclusions

In the current investigation, the following observations were concluded.

- A maximum RO16 dye removal of 92.30% was achieved by using biochar derived from *U. lactuca* at process conditions of biochar dosage of 2 g/L, pH of 2, initial concentration of 0.5 mmol/L, and temperature of 40°C.
- Characterization of biochar and dye bounded biochar showed that a major shift has been accrued in the functional groups.
- The predictive model of RSM and ANN was compared with the experimental trials and ANN was found to be the best fit model with a correlation coefficient (R^2) of 0.999.
- The statistical analysis of boxplot and HCA proved that ANN is the best predictive model for experimental trials in comparison with RSM predictive model.
- Furthermore, the response optimizer predicted that maximum removal of 93.52% can be obtained at a process condition of biochar dose of 3.33 g/L, pH of 3.53, and initial concentration of 0.46 mmol/L and temperature of 40°C.
- Adsorption isotherm and kinetic studies concluded that, the four-parameter model Fritz–Schlunder – IV and Marczewski–Jaroniec were found to best fit with a correlation coefficient of 0.9999 and pseudo-second-order kinetic model was found to be the best fit model with a correlation coefficient of not less than 0.9954.

References

[1] E. Forgacs, T. Cserhati, G. Oros, Removal of synthetic dyes from wastewaters: a review, Environ. Int., 30 (2004) 953–971.
[2] G. De Aragao Umbuzeiro, H.S. Freeman, S.H. Warren, D.P. de Oliveira, Y. Terao, T. Watanabe, L.D. Claxton, The contribution of azo dyes to the mutagenic activity of the Cristais River, Chemosphere, 60 (2005) 55–64.
[3] G. Crini, P.M. Badot, Application of chitosan, a natural amino polysaccharide, for dye removal from aqueous solutions by adsorption processes using bath studies: a review of recent literature, Prog. Polym. Sci., 33 (2008) 399–447.

[4] C.-Y. Chen, M.-C. Cheng, A.-H. Chen, Photocatalytic decolorization of Remazol Black 5 and Reactive Orange 16 by mesoporous TiO_2, J. Environ. Manage., 102 (2012) 125–133.
[5] R. Gokulan, G. Ganesh Prabhu, J. Jegan, A. Avinash, A critical insight into biomass derived biosorbent for remediation of dyes, Chemistryselect, 4 (2019) 9762–9775.
[6] O.S. Bello, T.T. Siang, M.A. Ahmad, Adsorption of Remazol Brilliant Violet-5R reactive dye from aqueous solution by cocoa pod husk-based activated carbon: kinetic, equilibrium and thermodynamic studies, Asia-Pac. J. Chem. Eng., 7 (2012) 378–388.
[7] A.U. Isah, G. Abdulraheem, S. Bala, S. Muhammad, M. Abdullahi, Kinetics, equilibrium and thermodynamics studies of C.I. Reactive Blue 19 dye adsorption on coconut shell based activated carbon, Int. Biodeterior. Biodegrad., 102 (2015) 265–273.
[8] M. Daoud, O. Benturki, Z. Kecira, P. Girods, A. Donnot, Removal of reactive dye (BEZAKTIV Red S-MAX) from aqueous solution by adsorption onto activated carbons prepared from date palm rachis and jujube stones, J. Mol. Liq., 243 (2017) 799–809.
[9] Y.S. Al-Degs, M.I. El-Barghouthi, A.H. El-Sheikh, G.M. Walker, Effect of solution pH, ionic strength, and temperature on adsorption behavior of reactive dyes on activated carbon, Dyes Pigm., 77 (2008) 16–23.
[10] L.C. Morais, O.M. Freitas, E.P. Gonçalves, L.T. Vasconcelos, C.G. González Beça, Reactive dyes removal from wastewaters by adsorption on eucalyptus bark: variables that define the process, Water Res., 33 (1999) 979–988.
[11] O.S. Bello, M.A. Ahmad, Adsorptive removal of a synthetic textile dye using cocoa pod husks, Toxicol. Environ. Chem., 93 (2011) 1298–1308.
[12] K.S. Low, C.K. Lee, K. Lee, Removal of reactive dyes by quaternized coconut husk, J. Environ. Sci. Health., Part A, 33 (1998) 1479–1489.
[13] T. Jóźwiak, U. Filipkowska, P. Bugajska, T. Kalkowski, The use of coconut shells for the removal of dyes from aqueous solutions, J. Ecol. Eng., 19 (2018) 129–135.
[14] J. Jegan, S. Praveen, T. B. Pushpa, R. Gokulan, Biodecolorization of basic violet 03 using biochar derived from agricultural wastes: isotherm and kinetics, J. Biobased Mater. Bioenergy, 14 (2020) 316–326.
[15] J. Jegan, S. Praveen, T. Bhagavathi Pushpa, R. Gokulan, Sorption kinetics and isotherm studies of cationic dyes using groundnut (*Arachis hypogaea*) shell derived biochar a low-cost adsorbent, Appl. Ecol. Environ. Res., 18 (2020) 1925–1939.
[16] I.L.C. Junior, L. Finger, P.P. Quitaiski, S.M. Neitzke, J.V. Besen, M.K. Correa, J.B.R. Mees, Biosorption of 5G blue reactive dye using waste rice husk, Ecletica Quim., 43 (2018) 45–58.
[17] S. Chakraborty, J.K. Basu, S. De, S. Dasgupta, Adsorption of reactive dyes from a textile effluent using sawdust as the adsorbent, Ind. Eng. Chem. Res., 45 (2006) 4732–4741.
[18] N. Priyantha, L.B.L. Lim, D.T.B. Tennakoon, E.T.Z. Liaw, C.H. Ing, A.B. Liyandeniya, Biosorption of cationic dyes on breadfruit (*Artocarpus altilis*) peel and core, Appl. Water Sci., 8 (2018) 1–11, doi: 10.1007/s13201-018-0648-3.
[19] H.I. Chienga, L.B.L. Lima, N. Priyantha, Enhancement of crystal violet dye adsorption on *Artocarpus camansi* peel through sodium hydroxide treatment, Desal. Water Treat., 58 (2017) 320–331.
[20] M.M. Hassan, C.M. Carr, A critical review on recent advancements of the removal of reactive dyes from dyehouse effluent by ion-exchange adsorbents, Chemosphere, 209 (2018) 201–219.
[21] P. Pengthamkeerati, T. Satapanajaru, N. Chatsatapattayakul, P. Chairattanamanokorn, N. Sananwai, Alkaline treatment of biomass fly ash for reactive dye removal from aqueous solution, Desalination, 261 (2010) 34–40.
[22] U. Filipkowska, Adsorption and desorption of reactive dyes onto chitin and chitosan flakes and beads, Adsorpt. Sci. Technol., 24 (2006) 781–795.
[23] M.E. Ignat, V. Dulman, T. Onofrei, Reactive red 3 and direct brown 95 dyes adsorption onto chitosan, Cellul. Chem. Technol., 46 (2012) 357–367.
[24] X. Jiang, Y. Sun, L. Liu, S. Wang, X. Tian, Adsorption of C.I. Reactive Blue 19 from aqueous solutions by porous particles of the grafted chitosan, Chem. Eng. J., 235 (2014) 151–157.
[25] N. Dizge, C. Aydiner, E. Demirbas, M. Kobya, S. Kara, Adsorption of reactive dyes from aqueous solutions by fly ash: kinetic and equilibrium studies, J. Hazard. Mater., 150 (2008) 737–746.
[26] S.C.R. Santos, V.J.P. Vilar, R.A.R. Boaventura, Waste metal hydroxide sludge as adsorbent for a reactive dye, J. Hazard. Mater., 153 (2008) 999–1008.
[27] E. Güneş, T. Kaygusuz, Adsorption of Reactive blue 222 onto an industrial solid waste included Al(III) hydroxide: pH, ionic strength, isotherms, and kinetics studies, Desal. Water Treat., 53 (2015) 2510–2517.
[28] M. Auta, B.H. Hameed, Optimized and functionalized paper sludge activated with potassium fluoride for single and binary adsorption of reactive dyes, J. Ind. Eng. Chem., 20 (2014) 830–840.
[29] M. Shirzad-Siboni, S.J. Jafari, O. Giahi, I. Kim, S.M. Lee, J.K. Yang, Removal of acid blue 113 and reactive black 5 dye from aqueous solutions by activated red mud, J. Ind. Eng. Chem., 20 (2014) 1432–1437.
[30] A. Geethakarthi, B.R. Phani Kumar, Adsorption of reactive dyes from aqueous solutions by tannery sludge developed activated carbon: kinetic and equilibrium studies, Int. J. Environ. Sci. Technol., 8 (2011) 561–570.
[31] L. Zhou, H. Zhou, Y. Hu, S. Yan, J. Yang, Adsorption removal of cationic dyes from aqueous solutions using ceramic adsorbents prepared from industrial waste coal gangue, J. Environ. Manage., 234 (2019) 245–252.
[32] M. El Hajam, N. Idrissi Kandri, A. Harrach, A. El khomsi, A. Zerouale, Adsorption of Methylene Blue on industrial softwood waste "Cedar" and hardwood waste "Mahogany": comparative study, Mater. Today: Proc., 13 (2019) 812–821.
[33] A. Vanaamudan, N. Pathan, P. Pamidimukkala, Adsorption of Reactive Blue 21 from aqueous solutions onto clay, activated clay, and modified clay, Desal. Water Treat., 52 (2014) 1589–1599.
[34] J.E. Aguiar, J.A. Cecilia, P.A.S. Tavares, D.C.S. Azevedo, E.R. Castellón, S.M.P. Lucena, I.J.J. Silva, Adsorption study of reactive dyes onto porous clay heterostructures, Appl. Clay Sci., 135 (2017) 35–44.
[35] A. Rahman, N. Kishimoto, T. Urabe, Adsorption characteristics of clay adsorbents - sepiolite, kaolin and synthetic talc - for removal of Reactive Yellow 138:1, Water Environ. J., 29 (2015) 375–382.
[36] T. Sismanoglu, Y. Kismir, S. Karakus, Single and binary adsorption of reactive dyes from aqueous solutions onto clinoptilolite, J. Hazard. Mater., 184 (2010) 164–169.
[37] S.L. Hii, L.L. Estrop, C.L. Wong, Adsorption of reactive blue 4 onto the chemically modified red seaweed *Amphiroa foliacea*: equilibrium, kinetics and modeling studies, Int. J. Phys. Sci., 6 (2011) 7171–7182.
[38] C. Liu, H. Yuan, J. Yang, B. Li, Effective biosorption of reactive blue 5 by pH-independent lyophilized biomass of *Bacillus megaterium*, Afr. J. Biotechnol., 10 (2011) 16626–16636.
[39] Z. Aksu, G. Donmez, A comparative study on the biosorption characteristics of some yeasts for Remazol blue reactive dye, Chemosphere, 50 (2003) 1075–1083.
[40] S.W. Won, S.B. Choi, B.W. Chung, D. Park, J.M. Park, Y.S. Yun, Biosorptive decolorization of Reactive orange 16 using the waste biomass of *Corynebacterium glutamicum*, Ind. Eng. Chem. Res., 43 (2004) 7865–7869.
[41] K. Vijayaraghavan, Y.S. Yun, Biosorption of C.I. Reactive Black 5 from aqueous solution using acid-treated biomass of brown seaweed *Laminaria* sp., Dyes Pigm., 76 (2008) 726–732.
[42] N. Saravanan, T. Kannadasan, C.A. Basha, V. Manivasagan, Biosorption of textile dye using immobilized bacterial (*Pseudomonas aeruginosa*) and fungal (*Phanerochate chrysosporium*) cells, Am. J. Environ. Sci., 9 (2013) 377–387.
[43] G. Bayramoglu, M. Çelik, Y. Arica, Biosorption of Reactive Blue 4 dye by native and treated fungus *Phanerocheate chrysosporium*: batch and continuous flow system studies, J. Hazard. Mater., 137 (2006) 1689–1697.

[44] T. Bhagavathi Pushpa, J. Jegan, S. Praveen, R. Gokulan, Biodecolorization of Basic Blue 41 using EM based composts: isotherm and kinetics, ChemistrySelect, 4 (2019) 10006–10012.
[45] T. O'Mahony, E. Guibal, J.M. Tobin, Reactive dye biosorption by *Rhizopus arrhizus* biomass, Enzyme Microb. Technol., 31 (2002) 456–463.
[46] R. Gokulan, G. Ganesh Prabhu, J. Jegan, A novel sorbent *Ulva lactuca*-derived biochar for remediation Reactive Orange 16 in packed column, Water Environ. Res., 91 (2019) 642–649.
[47] R. Gokulan, J. Raja Murugadoss, J. Jegan, A. Avinash, Comparative desorption studies on remediation of remazol dyes using biochar (sorbent) derived from green marine seaweeds, ChemistrySelect, 4 (2019) 7437–7445.
[48] R. Gokulan, A. Avinash, G.G. Prabhu, J. Jegan, Remediation of remazol dyes by biochar derived from *Caulerpa scalpelliformis* - an eco-friendly approach, J. Environ. Chem. Eng., 7 (2019) 103297, doi: 10.1016/j.jece.2019.103297.
[49] R. Gokulan, G. Ganesh Prabhu, A. Avinash, J. Jegan, Experimental and chemometric analysis of bioremediation of remazol dyes using biochar derived from green seaweeds, Desal. Water Treat., 184 (2020) 340–353.
[50] K. Vijayaraghavan, J. Jegan, Entrapment of brown seaweeds (*Turbinaria conoides* and *Sargassum wightii*) in polysulfone matrices for the removal of praseodymium ions from aqueous solutions, J. Rare Earth, 33 (2015) 1196–1203.
[51] J. Vijayaraghavan, T. Bhagavathi Pushpa, S.J. Sardhar Basha, K. Vijayaraghavan, J. Jegan, Evaluation of red marine alga *Kappaphycus alvarezii* as biosorbent for methylene blue: isotherm, kinetic, and mechanism studies, Sep. Sci. Technol., 50 (2015) 1120–1126.
[52] N. Marchitan, C. Cojocaru, A. Mereuta, G. Duca, I. Cretescu, M. Gonta, Modeling and optimization of tartaric acid reactive extraction from aqueous solutions: a comparison between response surface methodology and artificial neural network, Sep. Purif. Technol., 75 (2010) 273–285.
[53] U. Ecer, T. Sahan, A response surface approach for optimization of Pb(II) biosorption conditions from aqueous environment with *Polyporus squamosus* fungi as a new biosorbent and kinetic, equilibrium and thermodynamic studies, Desal. Water Treat., 102 (2018) 229–240.
[54] R.R. Karri, J.N. Sahu, Modeling and optimization by particle swarm embedded neural network for adsorption of zinc(II) by palm kernel shell based activated carbon from aqueous environment, J. Environ. Manage., 206 (2018) 178–191.
[55] A. Kausar, H.N. Bhatti, M. Iqbal, A. Ashraf, Batch versus column modes for the adsorption of radioactive metal onto rice husk waste: conditions optimization through response surface methodology, Water Sci. Technol., 76 (2017) 1035–1043.
[56] M.A. Bezerra, R.E. Santelli, E.P. Oliveira, L.S. Villar, L.A. Escaleira, Response surface methodology (RSM) as a tool for optimization in analytical chemistry, Talanta, 76 (2008) 965–977.
[57] R.H. Myers, D.C. Montgomery, Response Surface Methodology, John Wiley, New York, NY, 2002.
[58] A. Ghosh, P. Das, K. Sinha, Modeling of biosorption of Cu(II) by alkali modified spent tea leaves using response surface methodology (RSM) and artificial neural network (ANN), Appl. Water Sci., 5 (2015) 191–199.
[59] J. Behin, N. Farhadian, Response surface methodology and artificial neural network modeling of reactive red 33 decolorization by O_3/UV in a bubble column reactor, Adv. Environ. Technol., 1 (2016) 33–44.
[60] M. Taheri, M.R.A. Moghaddam, M. Arami, Optimization of acid black 172 decolorization by electrocoagulation using response surface methodology, Iran. J. Environ. Health Sci. Eng., 9 (2012) 1–8, doi: 10.1186/1735-2746-9-23.
[61] J.L. Pilkington, C. Preston, R.L. Gomes, Comparison of response surface methodology (RSM) and artificial neural networks (ANN) towards efficient extraction of artemisinin from *Artemisia annua*, Ind. Crops Prod., 58 (2014) 15–24.
[62] C.W. Zobel, D.F. Cook, Evaluation of neural network variable influence measures for process control, Eng. Appl. Artif. Intell., 24 (2011) 803–812.
[63] C.R. Alavala, Logic and Neural Networks: Basic Concepts and Applications, New Age Publications, India, 2007.
[64] P.E. Ohale, C.F. Uzoh, O.D. Onukwuli, Optimal factor evaluation for the dissolution of alumina from Azaraegbelu clay in acid solution using RSM and ANN comparative analysis, S. Afr. J. Chem. Eng., 24 (2017) 43–54.
[65] E. Betiku, S.S. Okunsolawo, S.O. Ajala, O.S. Odedele, Performance evaluation of artificial neural network coupled with generic algorithm and response surface methodology in modeling and optimization of biodiesel production process parameters from shea tree (*Vitellaria paradoxa*) nut butter, Renewable Energy, 76 (2015) 408–417.
[66] E. Betiku, S.O. Ajala, Modeling and optimization of *Thevetia peruviana* (yellow oleander) oil biodiesel synthesis via *Musa paradisiacal* (plantain) peels as heterogeneous base catalyst: a case of artificial neural network vs. response surface methodology, Ind. Crops Prod., 53 (2014) 314–322.
[67] R. Gokulan, G. Ganesh Prabhu, J. Jegan, Remediation of complex remazol effluent using biochar derived from green seaweed biomass, Int. J. Phytorem., 21 (2019) 1179–1189.
[68] A. Robic, C. Rondeau-Mouro, J.F. Sassi, Y. Lerat, M. Lahaye, Structure and interactions of ulvan in the cell wall of the marine green algae *Ulva rotundata* (Ulvales, Chlorophyceae), Carbohydr. Polym., 77 (2008) 206–216.
[69] Y. Chen, B. Wang, J. Xin, P. Sun, D. Wu, D, Adsorption behavior and mechanism of Cr(VI) by modified biochar derived from *Enteromorpha prolifera*, Ecotoxicol. Environ. Saf., 164 (2018) 440–447.
[70] Y. Zhao, D. Feng, Y. Zhang, Y. Huang, S. Sun, Effect of pyrolysis temperature on char structure and chemical speciation of alkali and alkaline earth metallic species in biochar, Fuel Process. Technol., 141 (2016) 54–60.
[71] S. Lim, K.T. Lee, Process intensification for biodiesel production from *Jatropha curcas* L. seeds: supercritical reactive extraction process parameters study, Appl. Energy, 103 (2013) 712–720.